JACS
JOURNAL OF THE AMERICAN CHEMICAL SOCIETY
Article
pubs.acs.org/JACS

Sliding-Ring Catenanes

Isurika R. Fernando,[†] Marco Frasconi,[†,§] Yilei Wu,[†,‡] Wei-Guang Liu,[⊥] Michael R. Wasielewski,[†,‡] William A. Goddard III,[⊥,#] and J. Fraser Stoddart*[,†]

[†]Department of Chemistry, Northwestern University, 2145 Sheridan Road, Evanston, Illinois 60208, United States
[§]Department of Chemical Sciences, University of Padova, Via Marzolo 1, Padova 35131, Italy
[‡]Argonne-Northwestern Solar Energy Research (ANSER) Center, Northwestern University, 2145 Sheridan Road, Evanston, Illinois 60208, United States
[⊥]Materials and Process Simulation Center, California Institute of Technology, Pasadena, California 91125, United States
[#]NanoCentury KAIST Institute and Graduate School of EEWS (WCU), Korea Advanced Institute of Science and Technology (KAIST), 373-1 Guseong Dong, Yuseong Gu, Daejeon 305-701, Republic of Korea

Supporting Information

ABSTRACT: Template-directed protocols provide a routine approach to the synthesis of mechanically interlocked molecules (MIMs), in which the mechanical bonds are stabilized by a wide variety of weak interactions. In this Article, we describe a strategy for the preparation of neutral [2]catenanes with sliding interlocked electron-rich rings, starting from two degenerate donor–acceptor [2]catenanes, consisting of a tetracationic cyclobis(paraquat-*p*-phenylene) cyclophane ($CBPQT^{4+}$) and crown ethers containing either (i) hydroquinone (HQ) or (ii) 1,5-dioxynaphthalene (DNP) recognition units and carrying out four-electron reductions of the cyclophane components to their neutral forms. The donor–acceptor interactions between the $CBPQT^{4+}$ ring and both HQ and DNP units present in the crown ethers that stabilize the [2]catenanes are weakened upon reduction of the cyclophane components to their radical cationic states and are all but absent in their fully reduced states. Characterization in solution performed by UV–vis, EPR, and NMR spectroscopic probes reveals that changes in the redox properties of the [2]catenanes result in a substantial decrease of the energy barriers for the circumrotation and pirouetting motions of the interlocked rings, which glide freely through one another in the neutral states. The solid-state structures of the fully reduced catenanes reveal profound changes in the relative dispositions of the interlocked rings, with the glycol chains of the crown ethers residing in the cavities of the neutral $CBPQT^{0}$ rings. Quantum mechanical investigations of the energy levels associated with the four different oxidation states of the catenanes support this interpretation. Catenanes and rotaxanes with sliding rings are expected to display unique properties.

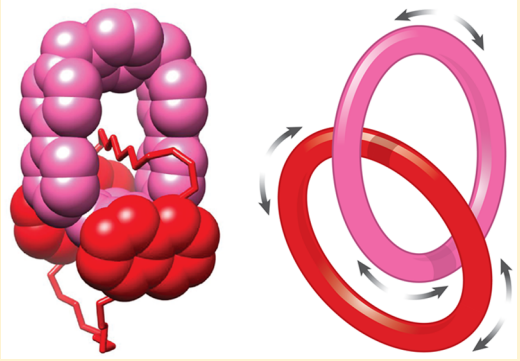

INTRODUCTION

Mechanically interlocked molecules[1] (MIMs), such as catenanes[2] and rotaxanes,[3] are an important class of compounds as a consequence of their unique physical, chemical, and electrochemical properties[4] which make them potential candidates for a wide range of applications,[5] including—but not limited to—providing switches for molecular electronic devices[6] and drug delivery systems.[7] In order to construct MIMs, template-directed protocols[8] that rely on, for example, (i) metal–ligand coordination,[9] (ii) aromatic donor–acceptor interactions,[10] (iii) hydrogen bonding,[11] (iv) anion coordination,[12] (v) radical–radical interactions,[13] (vi) halogen bonding,[14] and (vii) hydrophobic interactions[15] have been utilized widely. In particular, template-directed methodologies which rely upon donor–acceptor interactions[10] have emerged as some of the most extensively explored approaches for the synthesis of MIMs, following the introduction[16] of the electron-deficient tetracationic cyclophane, cyclobis(paraquat-*p*-phenylene) ($CBPQT^{4+}$), more than a quarter of a century ago. The molecular recognition that exists between the rigid, electron-deficient cavity of the $CBPQT^{4+}$ ring and the electron-rich cavities of aromatic crown ethers containing hydroquinone[17] (HQ) and 1,5-dioxynaphthalene[18] (DNP) units was exploited in the design and construction of the first generation of degenerate donor–acceptor catenanes.[19] Subsequently, the introduction[20] of an even better source of electron-donation in the form of electrochemically addressable tetrathiafulvalene (TTF) units led to the development[21,22] of a second generation of non-degenerate catenanes that exhibit externally governed, dual-mode, reversible switching of a $CBPQT^{4+}$ ring between TTF units and either HQ[21] or DNP[22] units present in the crown ether components of the catenanes.

Received: May 14, 2016
Published: July 11, 2016

DOI: 10.1021/jacs.6b04982
J. Am. Chem. Soc. 2016, 138, 10214–10225

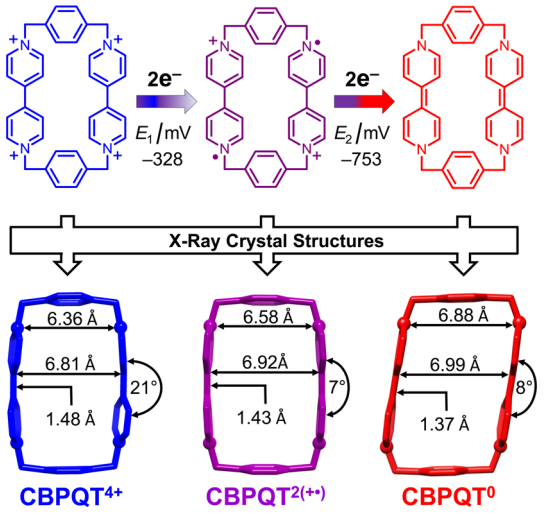

Figure 1. Structural formulas (top) and solid-state structures (bottom) of the cyclophane in its tetracationic $CBPQT^{4+}$ (blue), the diradical dicationic $CBPQT^{2(\bullet+)}$ (purple), and the fully neutral $CBPQT^{0}$ (red) forms. Plan view of the rings as tubular representations with distances, angles, and bond lengths, summarizing the rings' geometry in their three different oxidation states.

The chemistry of 1,1′-dialkyl-4,4′-bipyridinium ($BIPY^{2+}$) derivatives, especially the reduction and dimerization (pimerization) of the mono-reduced species $BIPY^{\bullet+}$, was explored in considerable detail by Kosower[23] and Hünig[24] in the 1960s. The electrochemical behavior of $CBPQT^{4+}$ is consistent[25] with the two $BIPY^{2+}$ units of the $CBPQT^{4+}$ ring being chemically equivalent and undergoing two consecutive reversible redox processes passing through a partially reduced diradical dicationic $CBPQT^{2(\bullet+)}$ on its way to a fully reduced neutral $CBPQT^{0}$ state. Thus, the diradical dicationic form and the neutral form of the cyclophane are comprised of two $BIPY^{\bullet+}$ and two $BIPY^{0}$ units, respectively. In more recent times, we have witnessed[26] the formation of a host–guest complex wherein the radical cation of the smallest $BIPY^{2+}$ derivative—namely, methyl viologen ($MV^{\bullet+}$)—becomes inserted into the cyclophane, forming a trisradical tricationic inclusion complex denoted by $CBPQT^{2(\bullet+)}\subset MV^{\bullet+}$. Following the identification of this strong 1:1 complex in solution as well as in the solid state, this inclusion complex has infiltrated many different aspects of supramolecular chemistry and mechanostereochemistry, including (i) the radical templation[13] of MIMs, (ii) the folding and unfolding of oligoviologens,[27] (iii) the extension and contraction of oligorotaxane radicals,[28] and (iv) the design and construction of artificial molecular pumps.[29]

Recently, we investigated the properties of the neutral $CBPQT^{0}$, the so-called red box,[25] by chemical reduction of the tetracationic $CBPQT^{4+}$, followed by extraction of the neutral species into an organic phase using an aqueous–organic biphasic procedure.[30,31] Following four-electron reduction, a change in the electronic properties of the $CBPQT^{4+}$ ring leads[25] to the binding of electron-poor substrates, such as 1,4-dicyanobenzene, in the electron-rich cavity of $CBPQT^{0}$. Additionally, a comparison of the solid-state structures of $CBPQT^{4+}$, $CBPQT^{2(\bullet+)}$, and $CBPQT^{0}$ reveals (Figure 1) a progressively wider cavity size, with [N···N′] distances ranging from 6.36 to 6.58 to 6.88 Å, respectively, while the [C4···C4′] distances increase from 6.81 to 6.92 to 6.99 Å, respectively. Moreover, the C4···C4′ bond distances associated with the $BIPY^{2(\bullet+)}$, $BIPY^{\bullet+}$, and $BIPY^{0}$ units decrease from 1.49 to 1.41 to 1.37 Å,

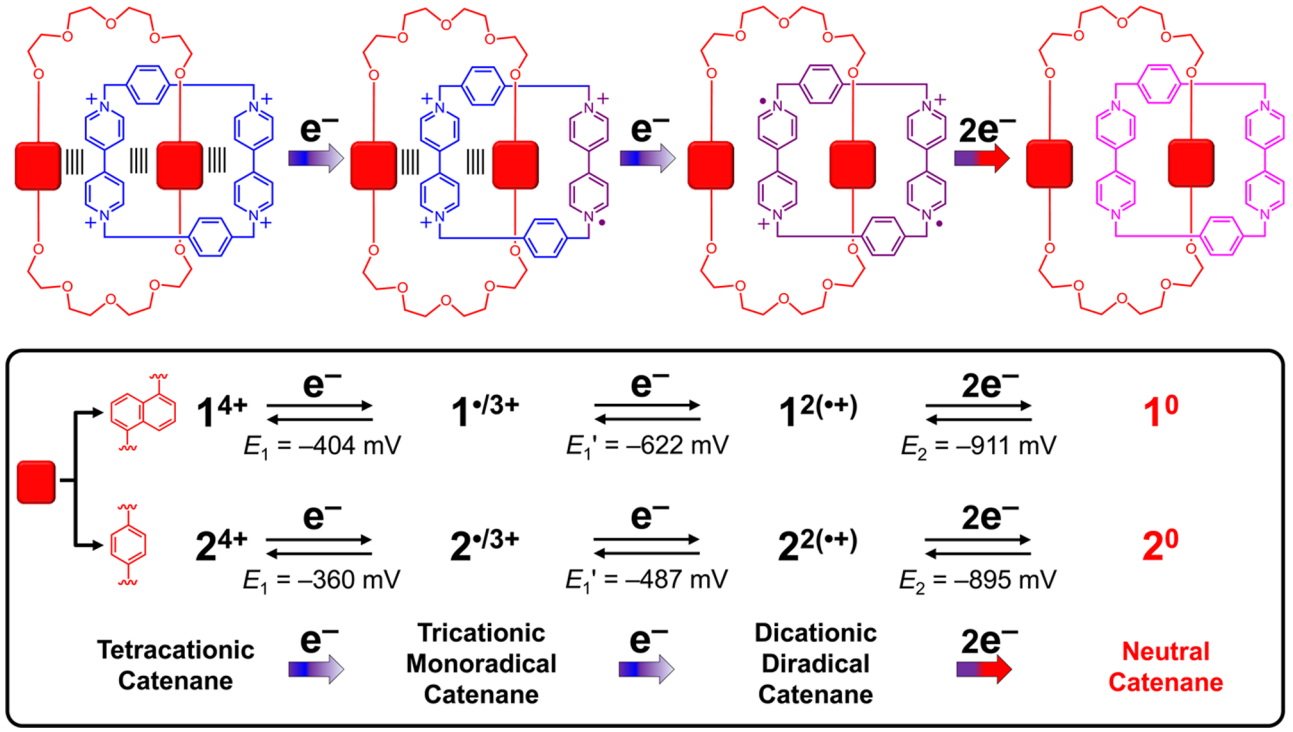

Figure 2. Schematic representation of the redox processes associated with the donor–acceptor [2]catenanes $\mathbf{1}^{4+}$ and $\mathbf{2}^{4+}$ comprising the redox-active $CBPQT^{4+}$ cyclophane and the DNP38C10 or BPP34C10 crown ether, respectively. Upon reduction, the fully charged species undergoes two consecutive reversible one-electron processes, affording the tricationic monoradical and the diradical dicationic states, followed by a third reduction involving two electrons, yielding the fully neutral catenane. The redox potentials were measured (see ref 18) in MeCN solution versus a SCE reference.

DOI: 10.1021/jacs.6b04982
J. Am. Chem. Soc. 2016, 138, 10214–10225

respectively, signifying a progressive loss of aromaticity. Dramatic changes in the stereoelectronic properties result from reversing electronically the role of the cyclophane from being a π-electron-deficient host, in its tetracationic form, to having an electron-rich cavity in the fully reduced CBPQT^0 state. This observation raises the question as to whether it might be possible to perturb the compact structures originating from the donor−acceptor interactions within the molecular frameworks of the first generation of degenerate donor−acceptor [2]catenanes in which bisparaphenylene-[34]crown-10[17,19,20] (BPP34C10) and 1,5-dinaphtho[38]crown-10[18,19,22] (DNP38C10) are both interlocked mechanically with CBPQT^{4+} rings. These tetracationic [2]catenanes undergo not two but three consecutive redox processes, leading to the identification (Figure 2), upon electrochemical reduction in solution, of tricationic monoradical and diradical dicationic catenanes, as well as fully neutral ones.

Here we present our detailed investigations of the structure−property relationships characteristic of the [2]catenanes DNP38C10/CBPQT (**1**) and BPP34C10/CBPQT (**2**) in their different redox states. Both experimental (in solution and in the solid state) and computational investigations were carried out. In an attempt to shed light on the nature of the molecular recognition between the mechanically interlocked rings in all four of their redox states, quantum mechanical calculations were performed. The partially charged (3+ and 2+) and the fully reduced neutral (0) states of [2]catenanes **1** and **2** in solution were accessed by chemical reduction of their oxidized 4+ states and characterized by UV−vis and continuous-wave electron paramagnetic resonance (EPR) spectroscopies. ^{1}H NMR spectra recorded for **1**^{0} and **2**^{0} in $CD_3C_6D_5$ at room temperature reveal line broadening of the resonances for the CBPQT^0 rings but not for the signals associated with the mechanically interlocked crown ethers, pointing to the existence of dynamic processes within the neutral catenanes. Finally, in order to elucidate the nature of the residual non-covalent bonding interactions between their mechanically interlocked electron-rich rings, single-crystal X-ray diffraction (XRD) analyses were performed on the neutral catenanes **1**^{0} and **2**^{0}.

EXPERIMENTAL SECTION

Materials and General Methods. All reagents were used as received from chemical suppliers (Aldrich and VWR), and reactions were carried out in anhydrous solvents under an inert N_2 atmosphere, unless otherwise stated. The compounds CBPQT·4PF$_6$,[16a,32] DNP38C10,[33] BPP34C10,[19,34] and the [2]catenanes,[18,19] **1**·4PF$_6$ and **2**·4PF$_6$, were all prepared according to previously reported literature procedures with minor modifications. Thin-layer chromatography (TLC) was performed on silica gel 60 F254 TLC plates (Merck), and chromatograms were viewed under UV light at either 256 or 354 nm. All samples employed in UV−vis, NMR, and EPR experiments were prepared inside an Ar-filled glovebox, and the measurements were carried out immediately following sample preparation. Solvents were degassed by purging with Ar gas for 2 h prior to transferring them to the glovebox. The different oxidation states, namely 3+, 2+, 1+, and 0, of **1**·4PF$_6$ and **2**·4PF$_6$ were obtained by adding 1.0, 2.0, 3.0, and 4.0 equiv, respectively, of cobaltocene to the solutions. Cobaltocene was assayed in dried and degassed MeCN using a colorimetric method[35] prior to the additions. In the cases of the UV−vis and EPR experiments, MeCN was used[36] as the solvent while NMR spectroscopic analyses were performed[37] in CD_3CN or $C_6D_5CD_3$. UV−vis spectra were obtained on a UV-3600 Shimadzu spectrophotometer. ^{1}H, ^{13}C, ROESY, DOSY, and variable-temperature (VT) NMR spectra were recorded on a Bruker Avance III instrument operating at 600 MHz for protons. The temperature (T) was calibrated using neat MeOH for T < 295 K and ethylene glycol for T > 295 K. Chemical shifts are referenced to the residual non-deuterated solvents—$C_6D_5CD_3$ at δ 2.09 ppm and CD_3CN at δ 1.94 ppm. EPR spectroscopic measurements were performed at room temperature using a Bruker Elexsys E580 X-Band (9.5 GHz) spectrometer outfitted with a variable Q splitting ring resonator (ER-4118X-MS5-W1). High-resolution mass spectra (HRMS) were recorded on an Agilent 6210 time-of-flight (TOF) LC-MS instrument employing an electrospray ionization (ESI) source coupled with an Agilent 1100 HPLC stack using direct infusion (0.6 mL min^{-1}). Single-crystal XRD analyses of the [2]catenanes in their 0 and 3+ oxidation states, i.e., **1**^{0}, **2**^{0}, **1**$^{\bullet/3+}$, and **2**$^{\bullet/3+}$ were performed on a Bruker Kappa Apex II CCD diffractometer using Cu Kα (λ = 0.15418 nm) radiation at 100 K. Structure solutions and refinements were carried out using the Olex 21.2 Suite[38] of programs. Data collection and structure refinement details are available in CIF files, corresponding to CCDC depositions 1479750, 1479752, 1479755, and 1479751. The supplementary crystallographic data for this manuscript can be obtained free of charge from www.ccdc.cam.ac.uk/data_request/cif.

Redox Titration. Cobaltocene was employed[39] as a reducing agent for the following reasons: (i) The redox potential of the $CoCp_2^+/CoCp_2$ couple is −0.89 V vs SCE, along with our recent investigations[25] which show that CBPQT^{4+} can be reduced by cobaltocene to its neutral oxidation state (CBPQT^0) without harm to the cyclophane. (ii) Since it is a single-electron reducing agent, oxidation states 3+, 2+, 1+, and 0 can be addressed precisely and achieved starting from the fully oxidized (4+) catenanes by adding 1.0, 2.0, 3.0, and 4.0 molar equiv of cobaltocene, respectively. (iii) Cobaltocene is readily soluble in a range of polar and apolar solvents, including pentane, PhMe, THF, CH_2Cl_2, Me_2CO, and MeCN. (iv) The reduction potential of the oxidized product—namely, the cobaltocenium ion—does not become involved in any side reactions. Reductions with cobaltocene were used in crystal growth experiments in addition to preparing samples for UV−vis and EPR spectroscopy.

UV−Vis Spectroscopy. A series of MeCN solutions with the catenanes in their 4+, 3+, 2+, 1+, and 0 redox states were prepared by reduction of the fully oxidized catenanes using 0.0, 1.0, 2.0, 3.0, and 4.0 molar equiv of cobaltocene, respectively. The entire range of spectra for the redox states of the catenanes with 1:0, 1:1, 1:2, 1:3, and 1:4 molar ratios of catenane:cobaltocene were recorded in a final volume of 1.0 mL using stock solutions of catenane (100 μM) and cobaltocene (1.7 mM). The concentration of catenanes **1**·4PF$_6$ and **2**·4PF$_6$ in MeCN was maintained at 100 μM in order to hold their optical densities below 1.5 using a standard 2 mm quartz cuvette.

EPR Spectroscopy. Samples were prepared as described for the UV−vis spectroscopic measurements with the exception that the concentration of the catenane stock solutions was maintained at 250 μM. All EPR spectra were recorded in MeCN at 298 K following reduction with cobaltocene.

NMR Spectroscopy. Samples of catenanes **1**^{0} and **2**^{0} were prepared as follows. The tetrachloride salts **1**·4Cl (12.0 mg, 7.3 μmol) and **2**·4Cl (10.0 mg, 8.3 μmol) were dissolved in an aqueous CO_3^{2-}/HCO^{3-} buffer (pH 8−9, 1.0 mL), and $CD_3C_6D_5$ (1 mL) was added to the buffered solution.[40] After activated Zn dust was added, the biphasic mixture was stirred at room temperature for 30 min. The initial color intensities of the aqueous layers—violet for **1**·4Cl and red for **2**·4Cl—decreased gradually while the colors of the $CD_3C_6D_5$ layers changed from colorless to light yellow, followed by the emergence of a dark yellowish-orange color, indicating that the neutral catenanes had been extracted into the $CD_3C_6D_5$ layers. The organic layers were washed with D_2O (3 × 1.0 mL), transferred to Wilmad NMR tubes, and capped. The caps on the NMR tubes were wrapped with parafilm to avoid oxidation of the neutral catenanes by air, and the NMR spectra were measured immediately thereafter.

^{1}H NMR data (600 MHz, $CD_3C_6D_5$, 298 K) for **1**^{0}: δ 8.02 (br, 4H, $H_{4/8}$), 7.20 (br, 4H, $H_{3/7}$), 7.10 (s, 8H, H_{Xy}), 6.47 (br, 4H, $H_{2/6}$), 5.28 (br, 8H, $H_{\alpha/\beta}$), 3.96 (br, OCH_{2a}), 3.60−3.55 (m, $OCH_{2b\text{-}d}$, N-CH_2).

^{1}H NMR data (600 MHz, $CD_3C_6D_5$, 298 K) for **2**^{0}: δ 7.22 (br, 8H, H_{Xy}), 6.57 (s, 8H, H_{HQ}), 5.43(br, 8H, H_α), 5.31 (br, 8H, H_β), 3.85 (t, J = 5.4 Hz, 8H, OCH_{2a}), 3.65 (br, 8H, N-CH_2), 3.57 (t, J = 5.4 Hz, 8H, OCH_{2b}), 3.53 (s, 16H, $OCH_{2c\text{-}d}$)

DOI: 10.1021/jacs.6b04982
J. Am. Chem. Soc. 2016, 138, 10214−10225

X-ray Crystallography. Unless otherwise stated, crystals of the [2]catenanes in their different redox states were grown under an atmosphere of Ar in a glovebox at 273 K.

For $\mathbf{1}^0$, a solution of $\mathbf{1}\cdot 4PF_6$ (4.75 mg, 2.7 mmol) in MeCN (1.00 mL) was treated with 5.0 equiv of a saturated cobaltocene solution (110 μL) in MeCN. The solution was filtered and left to stand for 1 h at room temperature; dark orange elongated single crystals of $\mathbf{1}^0$ were obtained.

Crystal data for $\mathbf{1}^0\cdot 2MeCN$ (C_{76} H_{82} N_6 O_{10}): M = 1239.47, monoclinic, space group $P12_1/c1$, a = 13.9493(8), b = 48.567(3), and c = 10.9451(5) Å, α = 90.00, β = 112.934(3), and γ = 90.00°, V = 6829.0(6) Å^3, T = 100.01 K, Z = 4, D_{calc} = 1.206 g cm^{-3}, μ(Cu Kα) = 0.642 mm^{-1}, reflections collected/unique = 20417/9824, observed reflections [$I > 2\sigma(I)$] = 6648, GOF (on F^2) = 1.067, $R(F)$, $R_w(F)$ [$I > 2\sigma(I)$] = 0.1095, 0.2433; CCDC No. 1479750.

For $\mathbf{2}^0$, a solution of $\mathbf{2}^0$ in PhMe was obtained using the biphasic extraction method[40] starting from $\mathbf{2}\cdot 4PF_6$ (5.0 mg, 3.0 mmol) as described for the NMR sample preparation. Diffusion of *n*-hexane vapor into a solution of $\mathbf{2}^0$ in PhMe yielded bright orange elongated crystals of $\mathbf{2}^0$.

Crystal data for $4(\mathbf{2}^0\cdot 1.5PhMe\cdot 0.25H_2O)$ (C_{298} H_{338} N_{16} O_{41}): M = 4799.82, triclinic, space group $P\bar{1}$, a = 20.1201(9), b = 26.1627(12), c = 26.4880(12) Å, α = 87.674(3), β = 69.262(2), γ = 78.983(3)°, V = 12793.9(10) Å^3, T = 100.01 K, Z = 2, D_{calc} = 1.246 g cm^{-3}, μ(Cu Kα) = 0.660 mm^{-1}, Reflections collected/unique 83250/43042, Observed reflections [$I > 2\sigma(I)$] = 27965, GOF (on F^2) 1.034, $R(F)$, $R_w(F)$ [$I > 2\sigma(I)$] = 0.0849, 0.2244; CCDC No. 1479752.

For $\mathbf{1}\cdot 3PF_6$, a solution of $\mathbf{1}\cdot 4PF_6$ (3.30 mg, 1.9 mmol) in MeCN (660 μL) was treated with activated Zn dust. After 30 min of stirring at room temperature, the suspension was filtered, and the filtrate was subjected to vapor diffusion with iPr$_2$O. Within 2 weeks, dark violet-purple needles of $\mathbf{1}\cdot 3PF_6$ were obtained.

Crystal data for $\mathbf{1}\cdot 3PF_6\cdot 2MeCN$ ($C_{76}H_{82}F_{18}N_6O_{10}P_3$): M = 1674.38, monoclinic, space group $C12/c$ 1, a = 21.9335(5), b = 13.4484(3), and c = 27.6224(6) Å, α = 90.00, β = 113.1366(7), and γ = 90.00°, V = 113.1366(7) Å^3, T = 100.01 K, Z = 4, D_{calc} = 1.484 g cm^{-3}, μ(Cu Kα) = 1.685 mm^{-1}, reflections collected/unique 56084/6377, observed reflections [$I > 2\sigma(I)$] = 6276, GOF (on F^2) 1.047, $R(F)$, $R_w(F)$ [$I > 2\sigma(I)$] = 0.0408, 0.1037; CCDC No. 1479755.

For $\mathbf{2}\cdot 3PF_6$, dark violet-purple needles of $\mathbf{2}\cdot 3PF_6$ were obtained following a procedure similar to that described for $\mathbf{1}\cdot 3PF_6$, except that $\mathbf{2}\cdot 4PF_6$ (3.50 mg, 2.1 mmol) was used at the outset.

Crystal data for $2(\mathbf{2}\cdot 3PF_6\cdot 5.5MeCN)$ ($C_{150}H_{177}F_{36}N_{19}O_{20}P_6$): M = 3435.92, monoclinic, space group $P12_1/n1$, a = 19.1189(5), b = 19.7795(6), and c = 45.0588(12) Å, α = 90.00, β = 93.421(2), and γ = 90.00°, V = 17009.2(8) Å^3, T = 100.01 K, Z = 4, D_{calc} = 1.342 g cm^{-3}, μ(Cu Kα) = 1.509 mm^{-1}, reflections collected/unique 128195/28831, observed reflections [$I > 2\sigma(I)$] = 22524, GOF (on F^2) 1.041, $R(F)$, $R_w(F)$ [$I > 2\sigma(I)$] = 0.0749, 0.2042; CCDC No. 1479751.

RESULTS AND DISCUSSION

In order to explore the properties of neutral BIPY units in confined environments and shed more understanding on the structure–property relationships in MIMs at different oxidation states, we have investigated two degenerate donor–acceptor [2]catenanes, $\mathbf{1}\cdot 4PF_6$ and $\mathbf{2}\cdot 4PF_6$, in which macrocyclic polyethers DNP38C10 and BPP34C10, respectively, are interlocked mechanically with $CBPQT^{4+}$ rings. Their syntheses rely on a template-directed protocol driven by $\pi\cdots\pi$ donor–acceptor and [C–H···O] interactions, as reported previously.[10a,18] As a consequence of intramolecular donor–acceptor charge transfer interactions transitions between the electron-rich DNP unit in $\mathbf{1}\cdot 4PF_6$ and the HQ unit in $\mathbf{2}\cdot 4PF_6$ and the electron-deficient $CBPQT^{4+}$, $\mathbf{1}\cdot 4PF_6$ is purple, while $\mathbf{2}\cdot 4PF_6$ is red, in the solid state.

Electrochemistry and UV–Vis Spectroscopy. The redox behavior of $\mathbf{1}\cdot 4PF_6$ and $\mathbf{2}\cdot 4PF_6$, as demonstrated[18] by cyclic voltammetry experiments in MeCN solution, indicates that the reduction of the interlocked $CBPQT^{4+}$ ring from the fully oxidized state (4+) involves two well-resolved single-electron reductions to reach, consecutively, the 3+ and 2+ oxidation states, followed by a two-electron reduction that leads to the fully reduced neutral form. The first one-electron process can be attributed to the reduction of the $BIPY^{2+}$ unit alongside the macrocyclic polyether, affording the tricationic monoradical catenane. The diradical dicationic state is formed upon reduction of the encircled $BIPY^{2+}$ unit, which is involved in strong donor–acceptor interactions. The two simultaneous one-electron reductions of the two spin-paired $BIPY^{\bullet+}$ units result in the production of the fully reduced (neutral) catenane. These processes occur for $\mathbf{1}\cdot 4PF_6$ and $\mathbf{2}\cdot 4PF_6$ at redox potentials of −911 and −895 mV, respectively, as measured[18] in MeCN solution versus a SCE reference. These reduction potentials are shifted to substantially more negative values, compared to the reduction potential of the diradical dicationic $CBPQT^{2(\bullet+)}$ going to the neutral $CBPQT^0$ ring, indicating some potential stabilization provided by the macrocyclic polyether toward the radical cationic $BIPY^{\bullet+}$ units of the $CBPQT^{2(\bullet+)}$ ring within the [2]catenanes.

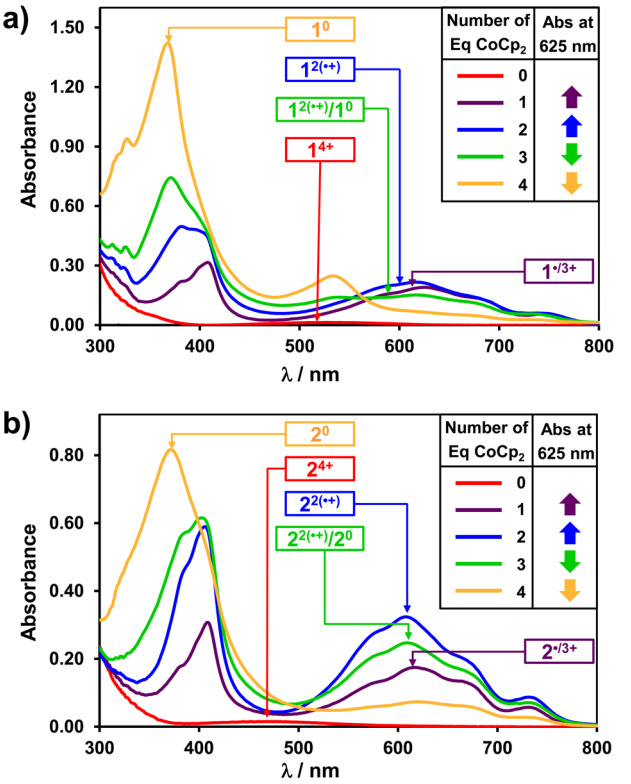

Figure 3. UV–vis absorption spectra of $\mathbf{1}\cdot 4PF_6$ (a) and $\mathbf{2}\cdot 4PF_6$ (b) recorded in Ar-purged MeCN solutions (100 μM) at 298 K along with their reduced states upon addition of 1.0, 2.0, 3.0, and 4.0 equiv of $CoCp_2$.

In an effort to explore the non-covalent bonding interactions occurring within the catenanes in their fully and partially charged forms, as well as in their neutral oxidation states, we isolated $\mathbf{1}\cdot 4PF_6$ and $\mathbf{2}\cdot 4PF_6$ in their different oxidation states and probed their physicochemical properties both in solution and in the solid state. The reduced forms of the catenane were generated by titrating solutions of $\mathbf{1}\cdot 4PF_6$ and $\mathbf{2}\cdot 4PF_6$ in MeCN with the chemical reductant cobaltocene ($CoCp_2$) under an atmosphere of Ar. The radical character of the catenanes in their different oxidation states in solution was probed by UV–vis and EPR

DOI: 10.1021/jacs.6b04982
J. Am. Chem. Soc. 2016, 138, 10214–10225

spectroscopies. The UV−vis spectra of **1**·4PF$_6$ (Figure 3a) and **2**·4PF$_6$ (Figure 3b) exhibit absorbance maxima at 530 and 470 nm, respectively. These absorption bands can be attributed to intramolecular charge-transfer transitions between the electron-rich DNP or HQ units of the crown ether and the electron-deficient BIPY^{2+} units of the CBPQT^{4+} ring in solution, as supported by DFT calculations (see the Supporting Information). Upon addition of 1.0 equiv of $CoCp_2$, the color of both catenane solutions changes to a dark blue which is characteristic of the radical cation, BIPY$^{\bullet+}$. This color change is accompanied by the emergence of two absorption bands in the UV−vis spectra at 418 and 620 nm. Following the stepwise addition of 2.0 equiv of $CoCp_2$ to the catenane solutions, the dark blue color intensifies and the absorbance of the radical cation bands nearly doubles. These two observations provide evidence for conversion of the remaining BIPY^{2+} units into the radical cationic BIPY$^{\bullet+}$ ones in both **1**·4PF$_6$ and **2**·4PF$_6$. In the presence of more than 2 equiv of the reductant, the color of both catenane solutions changes to bluish-green, and their UV−vis spectra show a decrease of the absorption band at 620 nm, while a new band emerges at 375 nm, indicating the formation of neutral BIPY^0 units. The fully reduced catenanes **1**^{0} and **2**^{0} are generated upon addition of 4.0 equiv of $CoCp_2$, as confirmed by the disappearance of the broad band at 620 nm and the concomitant increase of the band at 375 nm.

Solutions of the neutral catenanes **1**^{0} and **2**^{0} are stable under ambient conditions for more than 1 day prior to the slow reappearance of radical cationic bands in their UV−vis spectra. The intermediate radical cationic states, namely the tricationic monoradical and the diradical dicationic catenanes, are stable for several days under an Ar atmosphere while, upon exposure to air, they undergo oxidation much more readily when compared with their neutral counterparts.

EPR Spectroscopy. Continuous-wave (CW) EPR spectroscopy was performed in an effort to better understand the radical state of the catenanes at different oxidation states. Upon stepwise addition of the reducing agent to 250 μM solutions of catenanes **1**·4PF$_6$ and **2**·4PF$_6$, significant changes were observed in the EPR spectra in comparison with those of the fully oxidized catenanes, which are both EPR silent in their 4+ oxidation states. A gradual increase in the radical signal intensities, along with well-resolved hyperfine splitting patterns, was observed for the spectra of the tricationic monoradicals **1**$^{\bullet/3+}$ and **2**$^{\bullet/3+}$ as well as for the diradical dicationic **1**$^{2(\bullet+)}$ and **2**$^{2(\bullet+)}$, revealing the existence of a low-spin exchange regime for these oxidation states. The hyperfine splittings associated with **1**$^{\bullet/3+}$ and **2**$^{\bullet/3+}$ are similar to those commonly observed[41] for the radical cationic state of methyl viologen. The hyperfine structure disappears almost completely in the spectrum of **2**$^{2(\bullet+)}$ as a result of spin-exchange interactions between unpaired electrons in the two BIPY$^{\bullet+}$ units. In contrast, the reduction of **1**$^{\bullet/3+}$ to the diradical dicationic state **1**$^{2(\bullet+)}$ is accompanied by only a slight broadening of the hyperfine line compared with that observed in the EPR spectra of **2**$^{2(\bullet+)}$, a characteristic which is most likely the result of a reduced spin-exchange interaction on account of the "isolation" of the BIPY$^{\bullet+}$ units in **1**$^{2(\bullet+)}$. These subtly different observations suggest that the co-conformation with a π-electron-rich DNP unit located inside the CBPQT$^{2(\bullet+)}$ ring is favored. Addition of $CoCp_2$ up to 4.0 equiv results in the formation of the fully reduced catenanes, both of which are EPR silent (Figure 4).

NMR Spectroscopy. The diamagnetic character of the neutral catenanes **1**^{0} and **2**^{0} in solution means that they can be characterized by ^{1}H NMR spectroscopy, providing additional

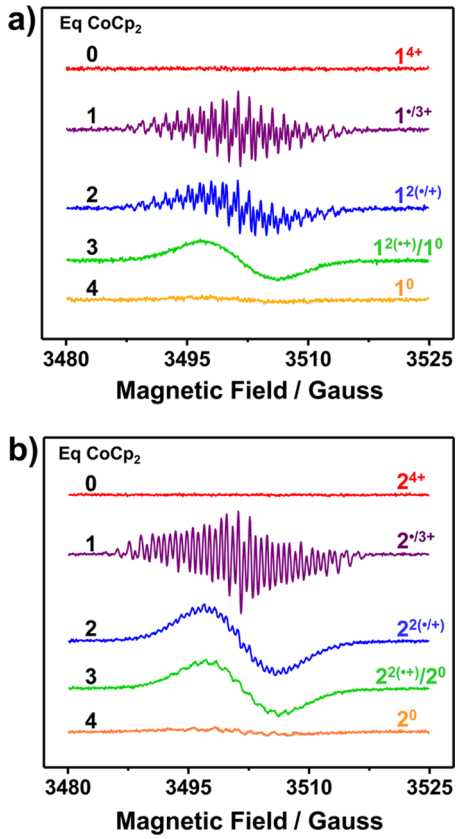

Figure 4. Continuous-wave EPR spectra of (a) **1**·4PF$_6$ and (b) **2**·4PF$_6$ (250 μM in MeCN at 298 K) and their reduced species obtained after addition of 1.0, 2.0, 3.0, and 4.0 equiv of $CoCp_2$ to Ar-purged MeCN solutions.

information about the nature of the non-covalent bonding interactions in these π-electron-rich neutral catenanes. As a consequence of the lack of donor−acceptor interactions upon chemical reduction, the molecular recognition between the fully neutral macrocycles—namely, the crown ether and CBPQT^0 ring—is presumably weakened to the extent that the relative circumrotation movements between the two interlocked rings are very much faster compared to other previously studied donor−acceptor catenanes. We have employed ^{1}H, ^{13}C, ROESY, and DOSY NMR spectroscopies to investigate the co-conformational behavior of both **1**^{0} and **2**^{0}. Solutions of these neutral catenanes for NMR characterization were prepared using an organic-aqueous biphasic extraction procedure[42] which was previously established by using different reducing agents to isolate the fully reduced methyl viologen. The procedure was developed[25] further by us during the isolation of the red box CBPQT^0. By employing this procedure, which takes advantage of the different solubilities of the fully oxidized (4+) and neutral (0) catenanes, **1**^{0} and **2**^{0} were extracted from aqueous solutions into $C_6D_5CD_3$ layers after being reduced to their neutral states using Zn dust in the alkaline aqueous phase under an atmosphere of Ar. Catenanes **1**^{0} and **2**^{0} display slightly different solubilities, with **2**^{0} being more soluble in $C_6D_5CD_3$ than **1**^{0}, most likely as a consequence of the compatibility of this solvent with the 1,4-dioxynapthalene units of the crown ether. Analysis by diffusion-ordered ^{1}H NMR spectroscopy (see Figures S4 and S5), performed on solutions of **1**^{0} and **2**^{0} following extraction into the $C_6D_5CD_3$ phase, confirmed the presence in solution of one species in each case. The ^{1}H NMR spectra of **1**^{0} and **2**^{0} reveal

DOI: 10.1021/jacs.6b04982
J. Am. Chem. Soc. 2016, 138, 10214−10225

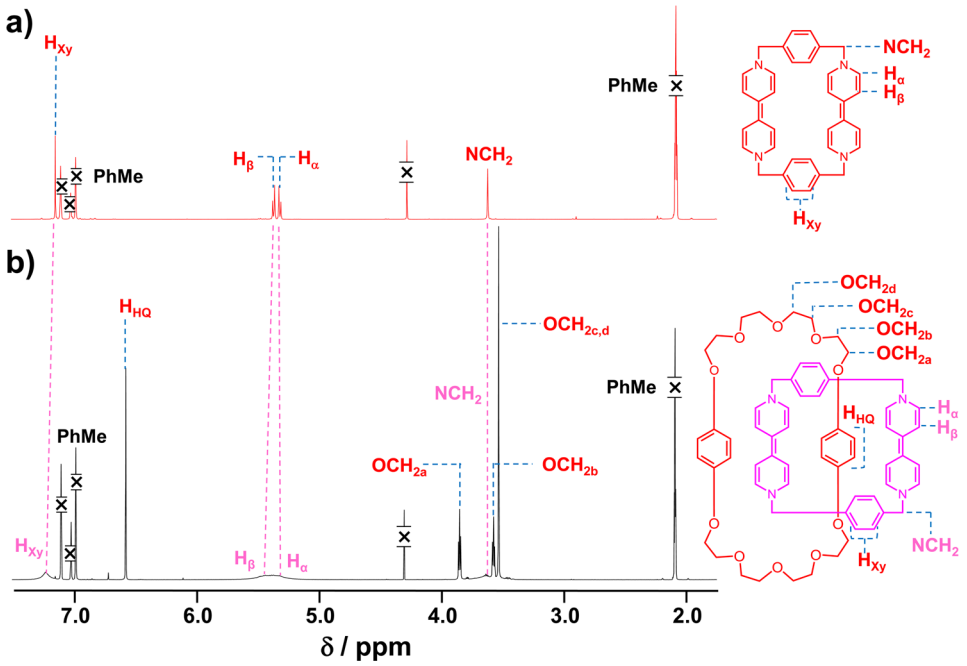

Figure 5. ^{1}H NMR spectra (600 MHz, $C_6D_5CD_3$, 298 K) of the neutral CBPQT^0 (a) and $\mathbf{2}^0$ (b). Assignments of the resonances of the neutral catenane have been confirmed with the assistance of data from 2D ^{1}H–^{1}H COSY experiments. See the Supporting Information.

shifts in the resonances of the protons in positions α and β to the nitrogens of the BIPY units corresponding to chemical shifts of around 5.43 and 5.36 ppm which are characteristic[25] of the neutral cyclophane CBPQT^0. These upfield shifts confirm the conversion of the BIPY units to nonaromatic planar constitutions as a result of their reduction to their neutral states. It is important to note that the resonances associated with the α and β protons, along with those for *N*-methylene (NCH_2) and phenylene (H_{Xy}) groups of the CBPQT ring in $\mathbf{1}^0$ and $\mathbf{2}^0$ are broadened (Figure 5) compared with those observed for the neutral cyclophane. This observation indicates the occurrence of dynamic bond rotation, presumably around the axis defined by the phenylene unit within the CBPQT^0 ring in solution at 298 K. In order to gain a better understanding of the dynamic nature of the neutral catenanes, variable-temperature ^{1}H NMR spectroscopy was carried out in $C_6D_5CD_3$ (Figures S2 and S3) over a range of temperatures from 203 to 373 K. Only one set of peaks were observed for the protons in $\mathbf{2}^0$ over the entire temperature range, commensurate with fast circumrotation of the BPP34C10 and CBPQT^0 rings occurring within the [2]catenane. By contrast, the ^{1}H NMR spectra of the fully oxidized $\mathbf{2}^{4+}$ in CD_3CN, measured for comparison over a 233 to 343 K temperature range, exhibit (Figure S3b) two sets of peaks for the inside and alongside protons of the HQ units, indicating that the crown ether undergoes slow exchange dynamics on the NMR time-scale within the temperature window of liquid CD_3CN. The observed coalescence temperature of 343 K at 600 MHz, along with the limiting chemical shift difference ($\Delta\nu$) of 1320 Hz between the two peaks for the slowly exchanging protons, allows a determination of the free energy of activation ($\Delta G_c^{\ddagger}$) of 61.6 kJ mol^{-1}. Although the DNP38C10 macrocyclic polyether places considerable geometric constraints on the $\mathbf{1}^0$ catenane with respect to $\mathbf{2}^0$, the presence of a single set of signals in the ^{1}H NMR spectrum of $\mathbf{1}^0$ in $C_6D_5CD_3$ (Figure S2) indicates that the dynamic processes between the interlocked electron-rich rings of these neutral catenanes remain fast on the ^{1}H NMR time-scale. Although the DNP38C10 macrocyclic polyether contains much larger aromatic units with respect to BPP34C10, the presence, once again, of only one single set of signals in the ^{1}H NMR spectrum of $\mathbf{1}^0$ in $C_6D_5CD_3$ (Figure S2) at room temperature indicates that the dynamic processes between the interlocked electron-rich rings of these neutral catenanes are still fast on the ^{1}H NMR time-scale. The proton resonances associated with the DNP38C10 ring of $\mathbf{1}^0$, however, separate out into two equal intensity resonances on cooling the solution below 263 K. By following the temperature dependence of the signals from the $H_{2/6}$ protons ($\Delta\nu$ = 150 Hz), a $\Delta G_c^{\ddagger}$ value of 12.3 kJ mol^{-1} was obtained, indicating an energy barrier which can be associated with the "flipping" of the DNP units. The resonances associated with the α and β protons of the neutral BIPY in $\mathbf{1}^0$ undergo broadening and coalescence at a temperature of 323 K, which is slightly higher than that observed for $\mathbf{2}^0$ as a result of a greater geometrical constraint imposed by the DNP38C10 as compared with the BPP34C10 ring.

X-ray Crystallography. The redox-controlled organization of the mechanically interlocked rings was revealed in the solid state by X-ray crystallographic analysis on single crystals of the catenanes in their different oxidation states. Reduction of the catenane $\mathbf{1}\cdot 4PF_6$ in MeCN with slightly more than 4 equiv of $CoCp_2$ yielded dark orange elongated single crystals in less than 1 h upon leaving the solution to stand in an atmosphere of Ar at room temperature. This observation is consistent with our recent results[25] obtained for CBPQT^0, where crystallization of the neutral box from a concentrated solution of the reduced form in MeCN resulted in dark reddish-orange cubes under the same conditions as those employed for growing crystals of $\mathbf{1}^0$. This case of crystallization is a result of the low solubility of the neutral species in polar solvents, such as MeCN. Orange crystals with the same unit cell were also obtained by slow vapor diffusion of iPr$_2$O into a dilute MeCN solution of the fully reduced catenane $\mathbf{1}^0$. The neutral state of the catenane is confirmed by the absence of counterions in the unit cell of the crystal, which is monoclinic and belongs to the $P2_1/c$ space group. The increased double bond character in the BIPY units as a consequence of the conversion of

DOI: 10.1021/jacs.6b04982
J. Am. Chem. Soc. 2016, 138, 10214–10225

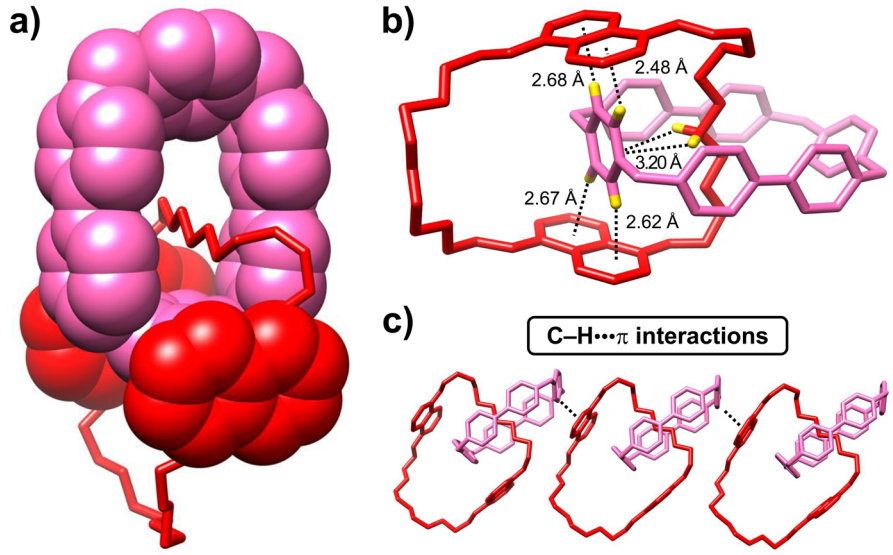

Figure 6. Solid-state (super)structure of the neutral $\mathbf{1}^0$ obtained from single-crystal X-ray crystallography. (a) Space-filling representation of the catenane from a perspective view, highlighting the encirclement of the neutral $CBPQT^0$ (pink) ring around the ethylene glycol chain of the DNP38C10 component (red) with both 1,5-dinaphtho units lying outside the ring. (b) Side-on view of catenane $\mathbf{1}^0$ in a tubular representation, showing the [CH···π] distances between the hydrogen atoms (yellow) of the polyether loop and the phenylene units of the ring. (c) Top view of the long-range packing of neutral catenanes represented in a tubular format showing the intermolecular [CH···π] interactions between the hydrogens of the phenylene rings in $CBPQT^0$ and the 1,5-dinaphtho units in the neighboring catenanes.

the aromatic pyridinum into dihydropyridine rings confirms that the conversion of the cyclophane to its neutral state was successful. After disrupting, by full reduction, the donor–acceptor interactions between the DNP units in DNP38C10 and the $BIPY^{2+}$ recognition sites in the $CBPQT^{4+}$ ring, the $CBPQT^0$ ring encircles (Figure 6a) the glycol chain of DNP38C10 in the solid-state structure of $\mathbf{1}^0$. Relocation of the $CBPQT^0$ ring within the catenane is governed by weak interactions (Figure 6b) that can be ascribed to two sets of factors. The first set includes edge-to-face aromatic [C–H···π] interactions between the alongside phenylene ring of the $CBPQT^0$ and the two DNP units in DNP38C10, which lie within a 2.62–2.48 Å distance range. The second set includes weak aliphatic [C–H···π] interactions emanating from the glycol chain of the crown ether and directed at a distance of 3.20 Å toward the phenylene group in the $CBPQT^0$ encircled by DNP38C10. Reduction of the cyclophane component to its uncharged state induces rotation of the phenylene group by almost 52° around the axis defined by the two methylene carbon atoms of $CBPQT^0$. As a result of this rotation, the phenylene group can become engaged (Figure 6c) in edge-to-face intermolecular [C–H···π] interactions (approximately 3.13–3.39 Å) with DNP units of the neighboring catenane. Intermolecular [C–H···O] interactions with a mean distance of 3.24–3.45 Å exist between the β protons of the BIPY units and the oxygen atoms of the crown ether of the neighboring catenane. In the crystal structure of fully oxidized $\mathbf{1}^{4+}$, intramolecular [C–H···O] interactions were observed[18] between the $CBPQT^{4+}$ ring and the ethylene glycol chain of the DNP38C10 ring.

In the case of the neutral catenane $\mathbf{2}^0$, bright-orange elongated single crystals were obtained by diffusion of *n*-hexane into a PhMe solution of $\mathbf{2}^0$, which was obtained by extraction from a heterogeneous two-phase system composed of PhMe and an alkaline aqueous layer. X-ray structural analysis of crystalline $\mathbf{2}^0$ revealed a triclinic unit cell with a $P\bar{1}$ space group displaying (Figure S8) four different co-conformations for the catenane $\mathbf{2}^0$. In all four co-conformations, the BPP34C10 ring's glycol chain is located in the cavity of the $CBPQT^0$ ring in an almost centrosymmetric fashion. In two of the co-conformations, the $CBPQT^0$ ring sits (Figure S9) on the first CH_2–O–CH_2 linker of the glycol chain, while, in the other two co-conformations, the ring is located around the second CH_2–O–CH_2 linker of the glycol chain. The strikingly different geometrical arrangement of the mechanically interlocked rings in the [2]catenane in its different oxidation states is highlighted in Figure 7, which depicts the solid-state structures of fully oxidized $\mathbf{2}^{4+}$ previously reported[18] (which we reproduce here for the sake of comparison) along with one of the co-conformations of the fully reduced $\mathbf{2}^0$ catenane. The loss of aromaticity by the BIPY units in their fully reduced states results in a co-conformational

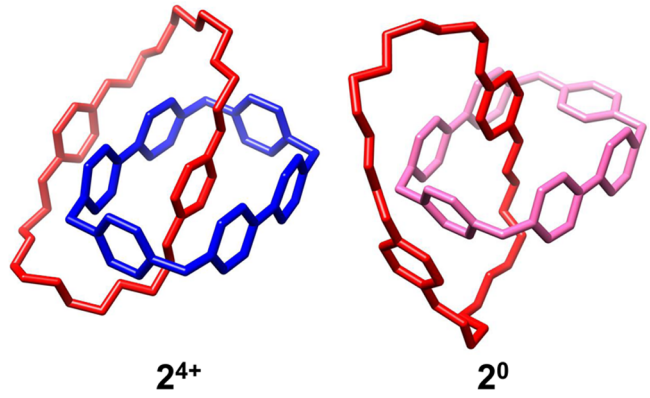

Figure 7. Solid-state structures of the fully oxidized $\mathbf{2}^{4+}$ and the neutral $\mathbf{2}^0$ in tubular representations displaying different interactions present in the catenanes, from an ordered donor–acceptor stack to a structure with a BPP34C10 ring that is capable of free movement with respect to the $CBPQT^0$ ring. The counterions, PF_6^-, have been omitted for the sake of clarity. Only one co-conformation of $\mathbf{2}^0$, which is present as four co-conformations in the solid state, is shown. See the Supporting Information.

DOI: 10.1021/jacs.6b04982
J. Am. Chem. Soc. 2016, 138, 10214–10225

change in the catenane. One of the HQ units in the BPP34C10 ring is situated alongside on the phenylene unit of the $CBPQT^0$ ring, separated by a plane-to-plane distance of 3.5 Å. Non-covalent bonding interactions help to sustain the other HQ unit located outside the cavity of the $CBPQT^0$ ring, resulting in edge-to-face [C–H···π] interactions between the HQ and the phenylene units. The co-conformations of these degenerate [2]catenanes—which are governed by donor–acceptor π-orbital overlap when the cyclophane component is in the fully oxidized state—change dramatically upon reduction of the $CBPQT^{4+}$ ring to its neutral $CBPQT^0$ form, resulting in a completely new set of non-covalent bonding interactions accompanied by very different molecular geometries contained within the same topology.

Geometrical changes within the cyclophane were also observed as a function of the oxidation state of the catenanes in the solid state. The geometrical parameters of the $CBPQT^0$ ring in $\mathbf{1}^0$ and $\mathbf{2}^0$ include (i) the dimension of the cavity, measured as a centroid-to-centroid distance between the planes of the two $BIPY^0$ units, and (ii) the torsion angle between the two rings in the $BIPY^0$ units. The geometries undergo significant changes when compared[25] with those observed for the "free" $CBPQT^0$. The encirclement of the $CBPQT^0$ ring around the glycol chain in the fully reduced [2]catenanes results in the "breathing" of the neutral cyclophane cavity. The breathing movements were confirmed by measuring the centroid-to-centroid distances between two parallel $BIPY^0$ units of $CBPQT^0$ that spans from 6.99 Å in empty $CBPQT^0$ to 7.37 and 7.70 Å in the case of the neutral catenanes $\mathbf{1}^0$ and $\mathbf{2}^0$, respectively.

The intermediate radical cationic states of each of the [2]catenanes—namely $\mathbf{1}^{\bullet/3+}$ and $\mathbf{2}^{\bullet/3+}$—were also investigated in the solid state. Upon addition of an excess of Zn dust to $\mathbf{1}\cdot 4PF_6$ and $\mathbf{2}\cdot 4PF_6$, the colors of the solutions change from the purple and red, characteristic of donor–acceptor charge transfer complexes, to dark blue, an indication that reduction of the $CBPQT^{4+}$ ring to the diradical dicationic form has taken place in solution. Slow vapor diffusion of $i Pr_2O$ into solutions of the reduced catenanes, following removal of the Zn dust under an atmosphere of Ar, afforded violet, elongated single cube-shape crystals suitable for XRD analysis.[43] The analysis revealed the presence of three PF_6^- counterions per catenane, indicating the adoption of tricationic monoradical states for these catenanes in the solid state even although UV–vis spectroscopic analysis of the initial catenane solutions revealed that the compounds had been reduced to their diradical dicationic states. This behavior, which was observed[44] previously during the crystallization of [2]catenanes containing radical cationic $BIPY^{\bullet+}$ units, could be the result of redox-mediated disproportionation during the crystallization of radical cationic species in nanoconfined environments. The solid-state structural analyses of $\mathbf{1}^{\bullet/3+}$ and $\mathbf{2}^{\bullet/3+}$ reveal (Figure 8) ordered molecular arrangements in which one of the DNP (or HQ) units is sandwiched between the BIPY components (mean interplanar distance of 3.4 Å), whist the other π-electron donor unit lies immediately adjacent to one of the BIPY units. The alongside BIPY unit of the $CBPQT^{\bullet/3+}$ exists in its radical cationic $BIPY^{\bullet+}$ form, as deduced from analyses of bond lengths and torsional angles, which is typical of radical cationic species. On the other hand, the dicationic $BIPY^{2+}$ units are located between the π-electron donor units of the macrocyclic polyethers, stabilized by donor–acceptor interactions with the two DNP (Figure 8b) and HQ (Figure 8d) units. The torsion angles for the radical cationic $BIPY^{\bullet+}$ and dicationic $BIPY^{2+}$ units are 7° and 10°, respectively, for $\mathbf{1}^{\bullet/3+}$. In the case of $\mathbf{2}^{\bullet/3+}$, the alongside $BIPY^{\bullet+}$ unit reveals a smaller torsional angle

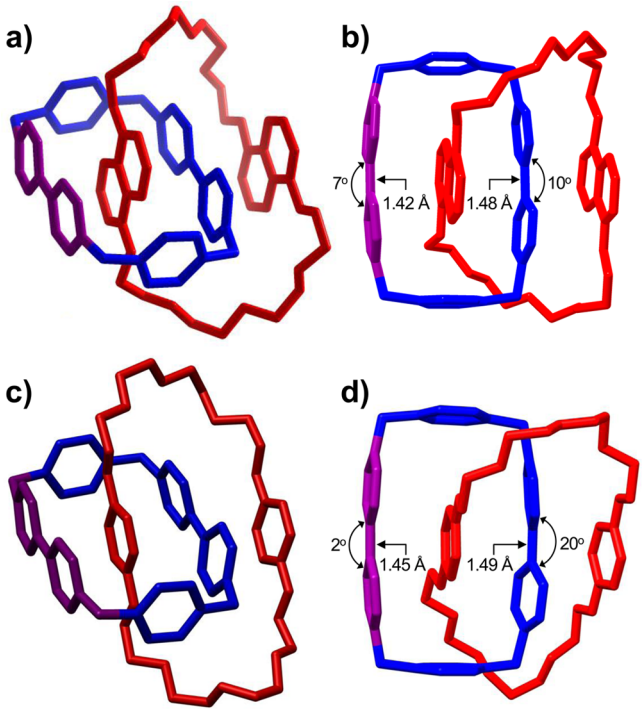

Figure 8. Perspective (a,c) and top (b,d) views employing tubular representations of the solid-state structures of $\mathbf{1}^{\bullet/3+}$ (a,b) and $\mathbf{2}^{\bullet/3+}$ (c,d). The bond lengths and the torsional angles associated with the alongside bipyridinium unit reflect its radical cationic nature, while the one encircled by two DNP or HQ units is in the dicationic state. The counterions, PF_6^-, have been omitted for the sake of clarity.

(2°) compared to that (20°) of the $BIPY^{2+}$ unit inside the DNP38C10 ring. An important influence of $BIPY^{\bullet+}$ on the structural properties of the catenanes is observed (Figure 9) in the extended solid-state superstructure of the $\mathbf{2}^{\bullet/3+}$ catenane. The packing in the crystal reveals an arrangement in which two $BIPY^{\bullet+}$ units of adjacent $\mathbf{2}^{\bullet/3+}$ catenanes undergo dimerization, with a centroid-to-centroid separation of 3.21 Å between the two $BIPY^{\bullet+}$ units of the $CBPQT^{\bullet/3+}$ rings. Weak [C–H···O] interactions are observed between the alongside HQ unit of one catenane and the second oxygen atoms in the polyether loop of a neighboring catenane. The superstructure of the catenane $\mathbf{2}^{\bullet/3+}$ in its tricationic monoradical form shows a packing with discrete domains of alternating radical–radical and donor–acceptor interactions. This superstructure confirms, along with previously reported[44a,45] bistable [2]rotaxanes, that the manipulation of the redox chemistry allows us to control these interactions beyond the molecule.

Quantum Mechanical Calculations. In order to examine the energies that govern the intramolecular non-covalent bonding interactions in the catenanes in their different oxidation states, density functional theory (DFT) was brought to bear on the problem. The initial geometries were taken from the crystal structures of the catenanes in their neutral (0) and fully oxidized (4+) states, wherein the cyclophane encircles the glycol chain and the π-electron donor groups, respectively. From these states the structures were relaxed[46] to the local minimum at the level of M06-HF/6-31G* with the Poisson–Boltzmann solvation model[47] (r_{probe} = 2.19 Å, ε = 37.5) to mimic the polarization in the condensed phase. The single-point energy was refined at the M06-HF/6-311++G** level. The high percentage of HF exchange helps the description of charge localization, which is

DOI: 10.1021/jacs.6b04982
J. Am. Chem. Soc. 2016, 138, 10214–10225

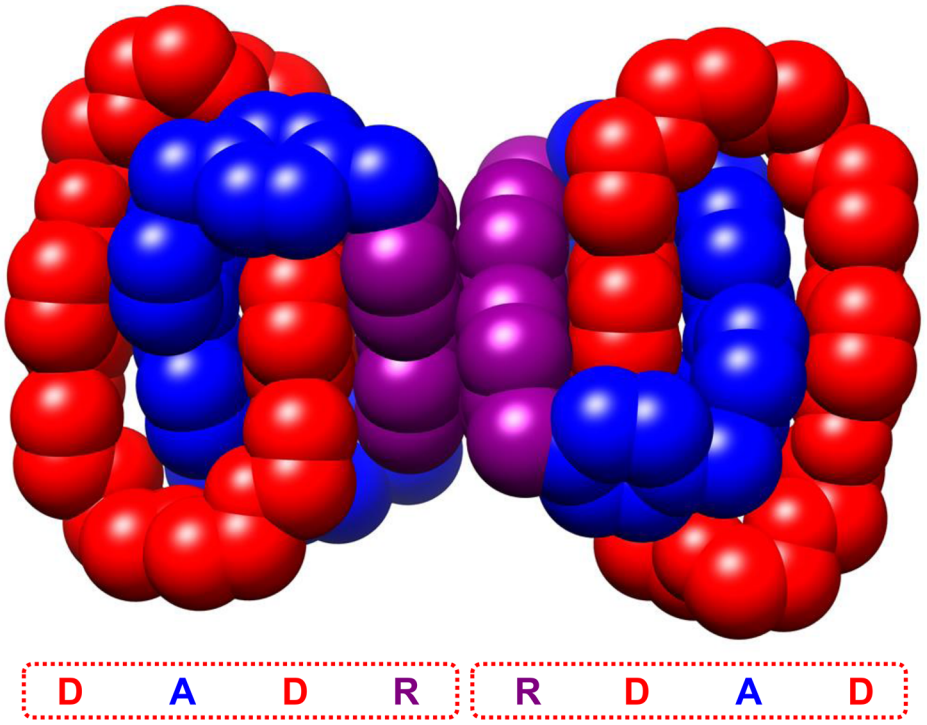

Figure 9. Solid-state superstructure of the $\mathbf{2}^{\bullet/3+}$ catenane in a space-filling representation showing the radical−radical $\pi\cdots\pi$ stacking interaction between the alongside $BIPY^{\bullet+}$ units of the catenanes. The face-to-face distance between the radical cations is 3.22 Å. The PF_6^- counterions and solvent molecules have been omitted for the sake of clarity.

important because of the drastic change in the oxidation state. The geometries predicted from the quantum mechanical calculations (Figure S10) carried out on catenanes $\mathbf{1}^{n+}$ and $\mathbf{2}^{n+}$ (n = 0, 3 and 4) are in agreement with the experimental observations. Comparison of the calculated structures with the solid-state crystal structures reveals similar positioning of $CBPQT^{n+}$ (n = 0−4) ring on the macrocyclic polyethers for both catenanes. Quantum mechanical calculations (Table 1) show that the two $BIPY^{2+}$ units of $CBPQT^{4+}$ in the catenane $\mathbf{1}^{4+}$ enter into a strong stabilizing interaction with the DNP units of the crown ether with 46.1 kcal mol^{-1} energy. Similarly, the $BIPY^{2+}$ units of the $CBPQT^{4+}$ ring reside on the HQ units of $\mathbf{2}^{4+}$ with 36.7 kcal mol^{-1} energy. This energy difference for the fully charged catenanes, $\mathbf{1}^{4+}$ and $\mathbf{2}^{4+}$, can be attributed to the strength of the donor−acceptor interactions between the DNP−$BIPY^{2+}$ couples compared with the HQ−$BIPY^{2+}$ recognition units. The DFT calculations show that, after reduction of $CBPQT^{4+}$ ring by one electron, the $CBPQT^{\bullet/3+}$ ring still prefers (although less so) to locate itself on the HQ or DNP units of the crown ether with the dicationic $BIPY^{2+}$ units residing inside the macrocyclic polyethers, stabilized by donor−acceptor interactions, as observed in the solid-state crystal structures of the catenanes $\mathbf{1}^{\bullet/3+}$ and $\mathbf{2}^{\bullet/3+}$. The co-conformation of $\mathbf{1}^{\bullet/3+}$ (Figure S11) with the dicationic $BIPY^{2+}$ unit positioned alongside the macrocyclic polyether and the radical cationic $BIPY^{\bullet+}$ unit residing inside the DNP38C10 ring results in a higher energy (5.0 kcal mol^{-1}) in comparison to the co-conformation that has the $BIPY^{2+}$ unit residing outside the macrocyclic polyether. Such a change in co-conformation in the case of the catenane $\mathbf{2}^{\bullet/3+}$ (Figure S12) does not occur because of the strong tendency of the dicationic unit to remain inside the macrocyclic polyether on account of stronger donor−acceptor and [C−H···O] interactions. The energy-optimized geometries (Figure S13) for the calculated structures of $\mathbf{1}^{2(\bullet+)}$ and $\mathbf{2}^{2(\bullet+)}$ show that, even after formation of the diradical dicationic $CBPQT^{2(\bullet+)}$, the $BIPY^{\bullet+}$ units encircle the aromatic units of the crown ethers. Interestingly, in the case of the calculated structure (Figure S14) of the catenane $\mathbf{1}^{\bullet+}$, the $CBPQT^{\bullet+}$ ring prefers (by 22.8 kcal mol^{-1}) to reside on the DNP unit rather than on the glycol chain, in stark contrast with the computed structure (Figure S15) for the catenane $\mathbf{2}^{\bullet+}$, in which the $CBPQT^{\bullet+}$ ring prefers (by 5.7 kcal mol^{-1}) to reside on the glycol chain. The distinctively different co-conformations adopted by these two catenanes result from the higher polarizability of DNP over HQ units, resulting in larger stabilization energies for the $CBPQT^{\bullet+}$ ring located on the DNP unit. The energy for the co-conformation obtained by switching the position of the radical cationic $BIPY^{\bullet+}$ unit of $\mathbf{1}^{\bullet+}$ from inside to alongside the DNP38C10 ring (Figure S14b) is 9.3 kcal mol^{-1} higher because of the lower polarization arising from the DNP units.

The calculated structures for the neutral catenanes $\mathbf{1}^0$ and $\mathbf{2}^0$ demonstrate that fully neutral CBPQT rings prefer to relocate along the glycol chain. In order to investigate the stability of the neutral catenanes in different co-conformations, we have calculated the potential energy surface for the sliding of the CBPQT ring through the crown ether and compared it with the energy for the movement of the $CBPQT^{4+}$ ring in the fully

Table 1. Calculated Energy Differences (A − B)[a] between the Co-conformations of CBPQT Residing on (A) the BPP/DNP Groups and (B) the Glycol Chain at Different Charge States

	charge on $CBPQT^{n+}$				
[2]catenane	4+	3+	2+	1+	0
$\mathbf{1}^{n+}$	−46.1	−40.6	−28.8	−22.8	0.5
$\mathbf{2}^{n+}$	−36.7	−29.4	−12.8	7.3	14.7

[a]Energy values in kcal mol^{-1}.

DOI: 10.1021/jacs.6b04982
J. Am. Chem. Soc. 2016, 138, 10214−10225

Table 2. Energy Decomposition Analysis of the Calculated Interaction Energies between the CBPQT Residing on the DNP Unit or the Glycol (GLY) Chain of the DNP38C10 Macrocycle at Different Charge States in a Vacuum[a]

	charge on $CBPQT^{n+}$									
catenane $\mathbf{1}^{n+}$	4+		3+		2+		1+		0	
location of CBPQT[b]	DNP	GLY	DNP	GLY	DNP	GLY	DNP	GLY	DNP	GLY
CEC[c]	−38.2	−20.8	−13.0	−4.5	−1.5	−3.2	13.5	6.3	38.7	15.2
PO[d]	−39.9	−30.0	−21.9	−18.0	−15.5	−11.7	−14.2	−8.1	−10.8	−5.4
CT[e]	−4.6	−3.0	−2.0	−2.2	−0.9	−1.0	−0.3	−0.3	1.0	0.2

[a]Calculated at the M06-HF/6-311G** level. Energy values in kcal mol^{-1}. [b]DNP: $CBPQT^{n+}$ ring encircles the DNP unit. GLY: $CBPQT^{n+}$ ring encircles the glycol chain. [c]Coulomb and exchange-correlation (CEC): frozen density component as in ref 48. [d]Polarization (PO): defined as the energy lowering due to the intramolecular relaxation of each molecule's absolutely localized MOs in the field of all other molecules in the system. [e]Charge-transfer (CT): defined as the energy lowering when the constraint of wave function localization is removed. The contribution from basis set superposition error is subtracted from this term.

oxidized catenanes. The neutral CBPQT ring encircling the DNP38C10 (or BPP34C10) crown ether was initially pushed away from the equilibrium position by 0.5 and 1.0 Å in the direction perpendicular to the plane defined by the carbons in four bismethylene units and then optimized with all the other coordinates relaxed. The potential energy surface is higher for both tetracationic catenanes $\mathbf{1}^{4+}$ and $\mathbf{2}^{4+}$ in comparison with the neutral catenanes (Figure S16). The higher energy cost calculated to move the $CBPQT^{4+}$ ring away from the equilibrium position for the catenanes in the 4+ charge state indicates a stronger interaction between the $CBPQT^{4+}$ ring and DNP (or HQ), an observation which is also reflected by the much greater stability (Table 1) of the co-conformations when the $CBPQT^{4+}$ ring encircles the aromatic units.

In order to elucidate the individual contributions of the interactions in the calculated catenane structures, we carried out the energy decomposition analysis (EDA) on different geometries and oxidation states of the $\mathbf{1}^{4+}$ catenane. This analysis was performed with absolutely localized molecular orbitals[48] at M06-HF/6-311G**, which allows the decomposition of the interaction energy into three terms: (i) Coulomb and exchange-correlation (CEC, also known as frozen density component), (ii) polarization (PO), and (iii) charge-transfer (CT). The results of the energy decomposition analysis, which are recorded in Table 2, highlight the individual contributions to the calculated differences in energy for the $\mathbf{1}^{4+}$ catenane at different oxidation states and in different co-conformations—namely, when the $CBPQT^{n+}$ ring encircles the DNP unit or the glycol (GLY) chain. The comparison between the energies calculated in this analysis, performed in vacuum, and the energies calculated in MeCN solution shows (Table 1) that, while the relative calculated energies are different, the overall trend of the stabilization energies from the positively charged catenane to the neutral catenane is similar. The results indicate that CEC and polarization interactions are the dominant contributors to the stabilization of the $CBPQT^{4+}$ ring and DNP38C10 in the fully oxidized catenanes. In the 4+ oxidation state, the CEC and polarization afford stabilization energies of 17.4 and 9.9 kcal mol^{-1}, respectively, for the $CBPQT^{4+}$ ring encircling the DNP unit. As the positive charge on the ring decreases, the driving force from CEC becomes less positive, and it assumes negative values for the oxidation state corresponding to the trisradical cationic catenane (1+). This trend can be explained by the increase in the electron-rich character of the system on reducing the oxidation state of the catenane and, therefore, causing an increase in the repulsion from Pauli exclusion. It is important to note that such an effect becomes significant in the case of the neutral CBPQT ring residing around the electron-rich DNP unit. Indeed, a driving force of 23.5 kcal mol^{-1} is calculated on moving the CBPQT ring from the DNP unit to the glycol chain and explains the tendency for the cyclophane in its lower oxidation states to encircle the glycol chain. The magnitude of polarization is also reduced as the charge becomes neutralized, but it always favors the binding between the DNP unit and the CBPQT ring. From this analysis, we conclude that the changes in co-conformations within these catenanes, achieved by varying their oxidation states, are determined by the interplay between polarization interactions and Pauli exclusion.

CONCLUSIONS

The redox-controlled structure−property relationships involving two degenerate donor−acceptor [2]catenanes have been characterized in both the solution and solid states by altering the redox state of the electron-poor cyclophane $CBPQT^{4+}$ component from its fully oxidized state (4+) to its fully reduced neutral (0) form, including the two intermediate states, namely 3+ and 2+. Single-crystal XRD analyses, along with solution-state investigations by UV−vis, EPR, and NMR spectroscopies, have revealed the non-covalent bonding interactions between the components of the [2]catenanes in their different oxidation states. Donor−acceptor interactions direct the assembly of the [2]catenanes, $\mathbf{1}^{4+}$ and $\mathbf{2}^{4+}$, and ensure the existence of ordered, compact structures which contain an alternating pattern of electron-rich units (DNP or HQ) and electron-deficient $BIPY^{2+}$ components. On reduction of the $CBPQT^{4+}$ ring to its neutral state, a drastically different situation pertains. The formation of the electron-rich $CBPQT^{0}$ ring within the molecular frameworks of these [2]catenanes results in the complete disruption of donor−acceptor interactions. Indeed, the isolation of neutral [2]catenanes comprising two electron-rich interlocked rings leads to the investigation of these MIMs from a different perspective. Our investigations demonstrate a complete change in the intramolecular interactions between the two interlocked rings such that, upon formation of the neutral species, the rings can glide freely through one another in solution, as confirmed by variable-temperature ^{1}H NMR spectroscopy. Single-crystal XRD analyses of the neutral catenanes $\mathbf{1}^{0}$ and $\mathbf{2}^{0}$ demonstrate that the glycol chains of the DNP38C10 and the BPP34C10 rings reside inside the cavity of the $CBPQT^{0}$ ring, while the electron-rich DNP and HQ units are located outside the cavity. This loss of molecular recognition results in completely different molecular geometries for the neutral catenanes in comparison with those of their fully oxidized states, despite their having the same topologies.

We have uncovered a strategy which allows access to catenanes—in good yields by template-directed protocols,

DOI: 10.1021/jacs.6b04982
J. Am. Chem. Soc. 2016, 138, 10214−10225

relying on either donor−acceptor or radical-pairing interactions—that afford, upon reduction of the cyclophane component to its neutral form, catenanes in which the molecular recognition between the two rings is exceedingly low. Access to catenanes with very low energy barriers to the gliding of their interlocked rings is important for the design and synthesis of artificial molecular machines.[29,49] Moreover, the extension of this concept into the realm of polyrotaxanes could lead[50] to novel sliding-ring materials under redox control with mechanical properties that could lead to applications as adhesives, coatings, and soft actuators.

■ ASSOCIATED CONTENT

Supporting Information

The Supporting Information is available free of charge on the ACS Publications website at DOI: 10.1021/jacs.6b04982.

Full details of instrumentation and materials and general methods; detailed NMR spectroscopic investigations of $\mathbf{1}^0$, $\mathbf{2}^0$, $\mathbf{1}^{4+}$, and $\mathbf{2}^{4+}$; solid-state characterization using XRD analysis; and quantum mechanical calculations, including Figures S1−S16 and Table S1 (PDF)

X-ray crystallographic analysis data for $\mathbf{1}^0$ (CIF)

X-ray crystallographic analysis data for $\mathbf{2}^0$ (CIF)

X-ray crystallographic analysis data for $\mathbf{1}^{\bullet/3+}$ (CIF)

X-ray crystallographic analysis data for $\mathbf{2}^{\bullet/3+}$ (CIF)

■ AUTHOR INFORMATION

Corresponding Author

*stoddart@northwestern.edu

Notes

The authors declare no competing financial interest.

■ ACKNOWLEDGMENTS

We thank Dr. Amy Sarjeant and Charlotte C. Stern for solving the single-crystal X-ray structures. This research is part of the Joint Center of Excellence in Integrated Nano-Systems (JCIN) at King Abdulaziz City for Science and Technology (KACST) and Northwestern University (NU). The authors would like to thank both KACST and NU for their continued support of this research. This work was also supported by the U.S. National Science Foundation (NSF) under grant no. CHE-1565925 (M.R.W.). W.A.G. gratefully acknowledges support (EFRI-1332411) from the NSF. Y.W. thanks the Fulbright Scholar Program for a Research Fellowship and gratefully acknowledges support from a Ryan Fellowship awarded by the NU International Institute for Nanotechnology (IIN).

■ REFERENCES

(1) (a) Schill, G. *Catenanes, Rotaxanes and Knots*; Academic Press: New York, 1971. (b) Dietrich-Buchecker, C.; Sauvage, J.-P. *Chem. Rev.* **1987**, *87*, 795−810. (c) Amabilino, D. B.; Stoddart, J. F. *Chem. Rev.* **1995**, *95*, 2725−2829. (d) Sauvage, J.-P., Dietrich-Buchecker, C., Eds. *Molecular Catenanes, Rotaxanes and Knots: A Journey Through the World of Molecular Topology*; Wiley: Weinheim, Germany, 1999. (e) Busch, D. *Top. Curr. Chem.* **2005**, *249*, 1−65. (f) Stoddart, J. F.; Colquhoun, H. M. *Tetrahedron* **2008**, *64*, 8231−8263. (g) Blanco, V.; Leigh, D. A.; Marcos, V. *Chem. Soc. Rev.* **2015**, *44*, 5341−5370.

(2) (a) Stoddart, J. F. *Angew. Chem., Int. Ed.* **2014**, *53*, 11102−11104. (b) Gil-Ramírez, G.; Leigh, D. A.; Stephens, A. J. *Angew. Chem., Int. Ed.* **2015**, *54*, 6110−6150.

(3) (a) Glink, P. T.; Schiavo, C.; Stoddart, J. F.; Williams, D. J. *Chem. Commun.* **1996**, 1483−1490. (b) Avestro, A.-J.; Belowich, M. E.; Stoddart, J. F. *Chem. Soc. Rev.* **2012**, *41*, 5881−5895. (c) Beves, J. E.; Blight, B. A.; Campbell, C. J.; Leigh, D. A.; McBurney, R. T. *Angew. Chem., Int. Ed.* **2011**, *50*, 9260−9327. (d) Bruns, C. J.; Stoddart, J. F. *Acc. Chem. Res.* **2014**, *47*, 2186−2199.

(4) (a) Choi, J.-W.; Flood, A. H.; Steuerman, D. W.; Nygaard, S.; Braunschweig, A. B.; Moonen, N. N.; Laursen, B. W.; Luo, Y.; DeIonno, E.; Peters, A. J.; Jeppesen, J. O.; Xu, K.; Stoddart, J. F.; Heath, J. R. *Chem. - Eur. J.* **2006**, *12*, 261−279. (b) Sun, J.; Wu, Y.; Wang, Z.; Liu, G.; Cheng, C.; Hartlieb, K. J.; Wasielewski, M. R.; Stoddart, J. F. *J. Am. Chem. Soc.* **2015**, *137*, 13484−13487.

(5) (a) Liu, Y.; Flood, A. H.; Bonvallet, P. A.; Vignon, S. A.; Northrop, B. H.; Tseng, H.-R.; Jeppesen, J. O.; Huang, T. J.; Brough, B.; Baller, B.; Magonov, S.; Solares, S. D.; Goddard, W. A., III; Ho, C.-M.; Stoddart, J. F. *J. Am. Chem. Soc.* **2005**, *127*, 9745−9759. (b) Berná, J.; Leigh, D. A.; Lubomska, M.; Mendoza, S. M.; Pérez, E. M.; Rudolf, P.; Teobaldi, G.; Zerbetto, F. *Nat. Mater.* **2005**, *4*, 704−710. (c) Fahrenbach, A. C.; Warren, S. C.; Incorvati, J. T.; Avestro, A.-J.; Barnes, J. C.; Stoddart, J. F.; Grzybowski, B. A. *Adv. Mater.* **2013**, *25*, 331−348.

(6) Coskun, A.; Spruell, J. M.; Barin, G.; Dichtel, W. R.; Flood, A. H.; Botros, Y. Y.; Stoddart, J. F. *Chem. Soc. Rev.* **2012**, *41*, 4827−4859.

(7) Fernando, I. R.; Ferris, D. P.; Frasconi, M.; Malin, D.; Strekalova, E.; Yilmaz, M. D.; Ambrogio, M. W.; Algaradah, M. M.; Hong, P. M.; Chen, X.; Nassar, M. S.; Botros, Y. Y.; Cryns, V. L.; Stoddart, J. F. *Nanoscale* **2015**, *7*, 7178−7183.

(8) (a) Anderson, S.; Anderson, H. L.; Sanders, J. K. M. *Acc. Chem. Res.* **1993**, *26*, 469−475. (b) Cacciapaglia, R.; Mandolini, L. *Chem. Soc. Rev.* **1993**, *22*, 221−231. (c) Raymo, F. M.; Stoddart, J. F. *Pure Appl. Chem.* **1996**, *68*, 313−322. (d) Breault, G. A.; Hunter, C. A.; Mayers, P. C. *Tetrahedron* **1999**, *55*, 5265−5293. (e) Hubin, T. J.; Busch, D. H. *Coord. Chem. Rev.* **2000**, *200*, 5−52. (f) Blanco, M.-J.; Chambron, J.-C.; Jiménez, M. C.; Sauvage, J.-P. *Top. Stereochem.* **2002**, *23*, 125−173. (g) Evans, N. H.; Beer, P. D. *Chem. Soc. Rev.* **2014**, *43*, 4658−4683.

(9) (a) Dietrich-Buchecker, C. O.; Sauvage, J.-P.; Kintzinger, J. P. *Tetrahedron Lett.* **1983**, *24*, 5095−5098. (b) Crowley, J. D.; Goldup, S. M.; Lee, A.-L.; Leigh, D. A.; McBurney, R. T. *Chem. Soc. Rev.* **2009**, *38*, 1530−1541.

(10) (a) Ashton, P. R.; Goodnow, T. T.; Kaifer, A. E.; Reddington, M. V.; Slawin, A. M. Z.; Spencer, N.; Stoddart, J. F.; Vicent, C.; Williams, D. J. *Angew. Chem., Int. Ed. Engl.* **1989**, *28*, 1396−1399. (b) Hamilton, D. G.; Davies, J. E.; Prodi, L.; Sanders, J. K. M. *Chem. - Eur. J.* **1998**, *4*, 608−620. (c) Barin, G.; Forgan, R. S.; Stoddart, J. F. *Proc. R. Soc. London, Ser. A* **2012**, *468*, 2849−2880.

(11) (a) Hunter, C. A. *J. Am. Chem. Soc.* **1992**, *114*, 5303−5311. (b) Vögtle, F.; Meier, S.; Hoss, R. *Angew. Chem., Int. Ed. Engl.* **1992**, *31*, 1619−1622. (c) Johnston, A. G.; Leigh, D. A.; Pritchard, R. J.; Deegan, M. D. *Angew. Chem., Int. Ed. Engl.* **1995**, *34*, 1209−1212. (d) Ashton, P. R.; Glink, P. T.; Stoddart, J. F.; Tasker, P. A.; White, A. J. P.; Williams, D. J. *Chem. - Eur. J.* **1996**, *2*, 729−736.

(12) (a) Lankshear, M. D.; Beer, P. D. *Acc. Chem. Res.* **2007**, *40*, 657−668. (b) Spence, G. T.; Beer, P. D. *Acc. Chem. Res.* **2013**, *46*, 571−586.

(13) (a) Li, H.; Fahrenbach, A. C.; Dey, S. V.; Basu, S.; Trabolsi, A.; Zhu, Z.; Botros, Y. Y.; Stoddart, J. F. *Angew. Chem., Int. Ed.* **2010**, *49*, 8260−8265. (b) Barnes, J. C.; Fahrenbach, A. C.; Cao, D.; Dyar, S. M.; Frasconi, M.; Giesener, M. A.; Benítez, D.; Tkatchouk, E.; Chernyashevskyy, O.; Shin, W. H.; Li, H.; Sampath, S.; Stern, C. L.; Sarjeant, A. A.; Hartlieb, K. J.; Liu, Z.; Carmieli, R.; Botros, Y. Y.; Choi, J.-W.; Slawin, A. M. Z.; Ketterson, J. B.; Wasielewski, M. R.; Goddard, W. A., III; Stoddart, J. F. *Science* **2013**, *339*, 429−433.

(14) Kilah, N. L.; Wise, M. D.; Serpell, C. J.; Thompson, A. L.; White, N. G.; Christensen, K. E.; Beer, P. D. *J. Am. Chem. Soc.* **2010**, *132*, 11893−11895.

(15) (a) Fujita, M.; Ibukuro, F.; Hagihara, H.; Ogura, K. *Nature* **1994**, *367*, 720−723. (b) Armspach, D.; Ashton, P. R.; Ballardini, R.; Balzani, V.; Godi, A.; Moore, C.; Spencer, N.; Stoddart, J. F.; Wear, T. J.; Williams, D. J.; Prodi, L.; Tolley, M. S.; Stoddart, J. F. *Chem. - Eur. J.* **1995**, *1*, 33−55. (c) Li, H.; Zhang, H.; Lammer, A. D.; Wang, M.; Li, X.; Lynch, V. M.; Sessler, J. L. *Nat. Chem.* **2015**, *7*, 1003−1008.

(16) (a) Odell, B.; Reddington, M. V.; Slawin, A. M. Z.; Spencer, N.; Stoddart, J. F.; Williams, D. J. *Angew. Chem., Int. Ed. Engl.* **1988**, *27*, 1547−1550. (b) Ashton, P. R.; Odell, B.; Reddington, M. V.; Slawin, A.

M. Z.; Stoddart, J. F.; Williams, D. J. *Angew. Chem., Int. Ed. Engl.* **1988**, *27*, 1550−1533.
(17) Brown, C. L.; Philp, D.; Stoddart, J. F. *Synlett* **1991**, *7*, 459−461.
(18) Ashton, P. R.; Brown, C. L.; Chrystal, E. J. T.; Goodnow, T. T.; Kaifer, A. E.; Parry, K. P.; Philp, D.; Slawin, A. M. Z.; Spencer, N.; Stoddart, J. F.; Williams, D. J. *J. Chem. Soc., Chem. Commun.* **1991**, 634−639.
(19) Anelli, P.-L.; Ashton, P. R.; Ballardini, B.; Balzani, V.; Delgado, M.; Gandolfi, M. T.; Goodnow, T. T.; Kaifer, A. E.; Philp, D.; Pietraszkiewicz, M.; Prodi, L.; Reddington, M. V.; Slawin, A. M. Z.; Spencer, N.; Stoddart, J. F.; Vicent, C.; Williams, C. J. *J. Am. Chem. Soc.* **1992**, *114*, 193−218.
(20) (a) Asakawa, M.; Ashton, P. R.; Balzani, V.; Credi, A.; Hamers, C.; Mattersteig, G.; Montalti, M.; Shipway, A. N.; Spencer, N.; Stoddart, J. F.; Tolley, M. S.; Venturi, M.; White, A. J. P.; Williams, D. J. *Angew. Chem., Int. Ed.* **1998**, *37*, 333−337. (b) Olson, M. A.; Botros, Y. Y.; Stoddart, J. F. *Pure Appl. Chem.* **2010**, *82*, 1569−1574.
(21) Asakawa, M.; Ashton, P. R.; Balzani, V.; Boyd, S. E.; Credi, A.; Mattersteig, G.; Menzer, S.; Montalti, M.; Raymo, F. M.; Ruffilli, C.; Stoddart, J. F.; Venturi, M.; Williams, D. J. *Eur. J. Org. Chem.* **1999**, *5*, 985−994.
(22) (a) Asakawa, M.; Higuchi, M.; Mattersteig, G.; Nakamura, T.; Pease, A. R.; Raymo, F. M.; Shimizu, T.; Stoddart, J. F. *Adv. Mater.* **2000**, *12*, 1099−1102. (b) Wang, C.; Cao, D.; Fahrenbach, A. C.; Fang, L.; Olson, M. A.; Friedman, D. C.; Basu, S.; Dey, S. K.; Botros, Y. Y.; Stoddart, J. F. *J. Phys. Org. Chem.* **2012**, *25*, 544−552.
(23) Kosower, E. M.; Cotter, J. L. *J. Am. Chem. Soc.* **1964**, *86*, 5524−5527.
(24) Hünig, S. *Pure Appl. Chem.* **1967**, *15*, 109−122.
(25) Frasconi, M.; Fernando, I. R.; Wu, Y.; Liu, Z.; Liu, W.-G.; Dyar, S. M.; Barin, G.; Wasielewski, M. R.; Goddard, W. A., III; Stoddart, J. F. *J. Am. Chem. Soc.* **2015**, *137*, 11057−11068.
(26) Trabolsi, A.; Khashab, N.; Fahrenbach, A. C.; Friedman, D. C.; Colvin, M. T.; Cotí, K. K.; Benítez, D.; Tkatchouk, E.; Olsen, J.-C.; Belowich, M. E.; Carmielli, R.; Khatib, H. A.; Goddard, W. A., III; Wasielewski, M. R.; Stoddart, J. F. *Nat. Chem.* **2010**, *2*, 42−49.
(27) Wang, Y.; Frasconi, M.; Liu, W.-G.; Liu, Z.; Nassar, M. S.; Botros, Y. Y.; Goddard, W. A., III; Stoddart, J. F.; Sarjeant, A. A. *J. Am. Chem. Soc.* **2015**, *137*, 876−885.
(28) Wang, Y.; Frasconi, M.; Liu, W.-G.; Sun, J.; Nassar, M. S.; Botros, Y. Y.; Goddard, W. A., III; Stoddart, J. F.; Wu, Y.; Wasielewski, M. R. *ACS Cent. Sci.* **2016**, *2*, 89−98.
(29) Cheng, C.; McGonigal, P. R.; Schneebeli, S. T.; Li, H.; Vermeulen, N. A.; Ke, C.; Stoddart, J. F. *Nat. Nanotechnol.* **2015**, *10*, 547−553.
(30) Carey, J. G.; Cairns, J. F.; Colchester, J. E. *J. Chem. Soc. D* **1969**, 1280−1281.
(31) Bockman, T. M.; Kochi, J. K. J. *J. Org. Chem.* **1990**, *55*, 4127−4135.
(32) Barnes, J. C.; Juríček, M.; Vermeulen, N. A.; Dale, E. J.; Stoddart, J. F. *J. Org. Chem.* **2013**, *78*, 11962−11969.
(33) Hamilton, D. G.; Davies, J. E.; Prodi, L.; Sanders, J. K. M. *Chem. - Eur. J.* **1998**, *4*, 608−620.
(34) Miljanić, O. Š.; Stoddart, J. F. *Proc. Natl. Acad. Sci. U. S. A.* **2007**, *104*, 12966−12970.
(35) Funston, A.; Kirby, J. P.; Miller, J. R.; Pospíšil, L.; Fiedler, J.; Hromadová, M.; Gál, M.; Pecka, J.; Valášek, M.; Zawada, Z.; Rempala, P.; Michl, J. *J. Phys. Chem. A* **2005**, *109*, 10862−10869.
(36) Characterization by UV−vis and EPR spectroscopy of the entire range of redox states occupied by the [2]catenanes from 4+ to 0 was carried out in MeCN because (i) the reducing agent, cobaltocene, (ii) the $4PF_6^-$ salts of the fully oxidized catenanes $\mathbf{1}^{4+}$ and $\mathbf{2}^{4+}$, and (iii) their partially reduced charged species, i.e., $\mathbf{1}^{\bullet/3+}$, $\mathbf{1}^{2(\bullet+)}$,$\mathbf{2}^{\bullet/3+}$, $\mathbf{2}^{2(\bullet+)}$, and $\mathbf{2}^{+/3\bullet}$, are readily soluble in MeCN, while (iv) the neutral catenanes $\mathbf{1}^0$ and $\mathbf{2}^0$ are also soluble in MeCN, albeit at low concentrations (0.25 mM).
(37) In an attempt to overcome the solubility issues and at the same time be able to use the same solvent for charged and neutral catenanes, the $4PF_6^-$ counterions of the fully oxidized catenanes were exchanged with apolar non-coordinating bulky counterions such as tetrakis[3,5-bis(trifluoromethyl)phenyl]borate and tetrakis(pentafluorophenyl)borate.
(38) Dolomanov, O. V.; Bourhis, L. J.; Gildea, R. J.; Howard, J. A. I.; Puschmann, H. *J. Appl. Crystallogr.* **2009**, *42*, 339−341.
(39) Connelly, N. G.; Geiger, W. E. *Chem. Rev.* **1996**, *96*, 877−910.
(40) Upon changing the pH of the aqueous medium from pH 7 to 8−9, the reduction potential of Zn of −0.76 V is decreased to −1.34 to −1.92 V. Since **1**·4Cl and **2**·4Cl are readily soluble in H_2O and stable in aqueous CO_3^{2-}/HCO_3^- buffer at pH 8−9, the reduction potential of $\mathbf{1}^{4+}$ and $\mathbf{2}^{4+}$ going to the neutral state can be reached in this buffer using activated Zn as the reducing agent. Also, since $\mathbf{1}^0$ and $\mathbf{2}^0$ are completely insoluble in H_2O (D_2O), they can be extracted into $C_6D_5CD_3$ prior to recording their NMR spectra.
(41) Gaudiello, J. G.; Ghosh, P. K.; Bard, A. J. *J. Am. Chem. Soc.* **1985**, *107*, 3027−3032.
(42) Maidan, R.; Goren, Z.; Becker, J. Y.; Willner, I. *J. Am. Chem. Soc.* **1984**, *106*, 6217−6222.
(43) Freshly generated crystals of $\mathbf{1}\cdot 3PF_6$ and $\mathbf{2}\cdot 3PF_6$ are stable for almost 12 h under ambient conditions. After this time, a decrease in intensity of the color of the crystals is observed, and the solids become colorless in one day. In comparison to other crystals containing bipyridinium radical cations, that have shorter lifetimes, the stability of the radical species of the tetracationic monoradical catenanes is achieved by the close packing of the BIPY units within the catenane framework.
(44) (a) Fahrenbach, A. C.; Zhu, Z. X.; Cao, D.; Liu, W. G.; Li, H.; Dey, S. K.; Basu, S.; Trabolsi, A.; Botros, Y. Y.; Goddard, W. A., III; Stoddart, J. F. *J. Am. Chem. Soc.* **2012**, *134*, 16275−16288. (b) Barin, G.; Frasconi, M.; Dyar, S. M.; Iehl, J.; Buyukcakir, O.; Sarjeant, A. A.; Carmieli, R.; Coskun, A.; Wasielewski, M. R.; Stoddart, J. F. *J. Am. Chem. Soc.* **2013**, *135*, 2466−2469.
(45) Zhu, Z.; Fahrenbach, A. C.; Li, H.; Barnes, J. C.; Liu, Z.; Dyar, S. M.; Zhang, H.; Lei, J.; Carmieli, R.; Sarjeant, A. A.; Stern, C. L.; Wasielewski, M. R.; Stoddart, J. F. *J. Am. Chem. Soc.* **2012**, *134*, 11709−11720.
(46) Zhao, Y.; Truhlar, D. G. *J. Phys. Chem. A* **2006**, *110*, 13126−13130.
(47) Tannor, D. J.; Marten, B.; Murphy, R.; Friesner, R. A.; Sitkoff, D.; Nicholls, A.; Ringnalda, M.; Goddard, W. A., III; Honig, B. *J. Am. Chem. Soc.* **1994**, *116*, 11875−11882.
(48) Khaliullin, R. Z.; Cobar, E. A.; Lochan, R. C.; Bell, A. T.; Head-Gordon, M. *J. Phys. Chem. A* **2007**, *111*, 8753−8765.
(49) (a) Li, H.; Cheng, C.; McGonigal, P. R.; Fahrenbach, A. C.; Frasconi, M.; Liu, W.-G.; Zhu, Z.; Zhao, Y.; Ke, C.; Lei, J.; Young, R. M.; Dyar, S. M.; Co, D. T.; Yang, Y. W.; Botros, Y. Y.; Goddard, W. A., III; Wasielewski, M. R.; Astumian, R. D.; Stoddart, J. F. *J. Am. Chem. Soc.* **2013**, *135*, 18609−18620. (b) McGonigal, P. R.; Li, H.; Cheng, C.; Schneebeli, S. T.; Frasconi, M.; Witus, L. S.; Stoddart, J. F. *Tetrahedron Lett.* **2015**, *56*, 3591−3594. (c) Cheng, C.; McGonigal, P. R.; Stoddart, J. F.; Astumian, R. D. *ACS Nano* **2015**, *9*, 8672−8688. (d) Cheng, C.; Stoddart, J. F. *ChemPhysChem* **2016**, *17*, 1780−1793.
(50) (a) Kato, K.; Yasuda, T.; Ito, K. *Macromolecules* **2013**, *46*, 310−316. (b) Bin Imran, A.; Esaki, K.; Gotoh, H.; Seki, T.; Ito, K.; Sakai, Y.; Takeoka, Y. *Nat. Commun.* **2014**, *5*, 5124.

DOI: 10.1021/jacs.6b04982
J. Am. Chem. Soc. 2016, 138, 10214−10225